



HHS Public Access

Author manuscript

Nucl Med Biol. Author manuscript; available in PMC 2015 October 28.

Published in final edited form as:

Nucl Med Biol. 2015 October ; 42(10): 780–787. doi:10.1016/j.nucmedbio.2015.06.003.

A high-affinity [¹⁸F]-labeled phosphoramidate peptidomimetic PSMA-targeted inhibitor for PET imaging of prostate cancer

Tanushree Ganguly^{a,1}, Shorouk Dannoon^{b,1}, Mark R. Hopkins^a, Stephanie Murphy^b, Hendry Cahaya^b, Joseph E. Blecha^b, Salma Jivan^b, Christopher R. Drake^b, Cyril Barinka^c, Ella F. Jones^{b,2}, Henry F. VanBrocklin^{b,2}, and Clifford E. Berkman^{a,d,*,2}

^aDepartment of Chemistry, Washington State University, USA

^bDepartment of Radiology and Biomedical Imaging, University of CA, San Francisco, USA

^cInstitute of Biotechnology, CR, Prague

^dCancer Targeted Technology, USA

Abstract

Introduction—In this study, a structurally modified phosphoramidate scaffold, with improved prostate-specific membrane antigen (PSMA) avidity, stability and *in vivo* characteristics, as a PET imaging agent for prostate cancer (PCa), was prepared and evaluated.

Methods—*p*-Fluorobenzoyl-aminohexanoate and 2-(3-hydroxypropyl)glycine were introduced into the PSMA-targeting scaffold yielding phosphoramidate 5. X-ray crystallography was performed on the PSMA/5 complex. [¹⁸F]5 was synthesized, and cell uptake and internalization studies were conducted in PSMA(+) LNCaP and CWR22Rv1 cells and PSMA(−) PC-3 cells. *In vivo* PET imaging and biodistribution studies were performed at 1 and 4 h post injection in mice bearing CWR22Rv1 tumor, with or without blocking agent.

Results—The crystallographic data showed interaction of the *p*-fluorobenzoyl group with an arene-binding cleft on the PSMA surface. *In vitro* studies revealed elevated uptake of [¹⁸F]5 in PSMA(+) cells (2.2% in CWR22Rv1 and 12.1% in LNCaP) compared to PSMA(−) cells (0.08%) at 4 h. *In vivo* tumor uptake of 2.33% ID/g and tumor-to-blood ratio of 265:1 was observed at 4 h.

Conclusions—We have successfully synthesized, radiolabeled and evaluated a new PSMA-targeted PET agent. The crystal structure of the PSMA/5 complex highlighted the interactions within the arene-binding cleft contributing to the overall complex stability. The high target uptake and rapid non-target clearance exhibited by [¹⁸F]5 in PSMA(+) xenografts substantiates its potential use for PET imaging of PCa.

Advances in Knowledge—The only FDA-approved imaging agent for PCa, Proscint®, targets PSMA but suffers from inherent shortcomings. The data acquired in this manuscript

*Corresponding author at: Washington State University, Department of Chemistry, Pullman, WA 99164–4630. Tel.: +1 509 335 7613; fax: +1 509 335 8389. cberkman@wsu.edu (C.E. Berkman).

¹Contributed equally.

²Contributed equally as senior authors.

Conflict of interest

The authors declare that they have no conflict of interest.

confirmed that our new generation of [^{18}F]-labeled PSMA inhibitor exhibited promising *in vivo* performance as a PET imaging agent for PCa and is well-positioned for subsequent clinical trials.

Implications for Patient Care—Our preliminary data demonstrate that this tracer possesses the required imaging characteristics to be sensitive and specific for PCa imaging in patients at all stages of the disease.

Keywords

Flourine-18; PET; PSMA; Phosphoramidate

1. Introduction

Owing to its unique and ubiquitous expression in prostate cancers (PCa) with limited (100–1000 fold lower) expression in other organs, prostate-specific membrane antigen (PSMA) is an ideal biomarker [1] and has attracted significant attention as a target for imaging [2–7] and treatment of PCa [8–10].

The only FDA-approved single-photon emission computed tomography (SPECT) diagnostic imaging agent for PCa, Prostascint®, an ^{111}In -labeled antibody that recognizes an intracellular epitope of the PSMA transmembrane protein [11], is only accessible in damaged or necrotic prostate tumor cells. Even though other antibodies targeted to extracellular epitopes of PSMA have been employed successfully to deliver diagnostic and therapeutic radionuclides [3,12–14], the long accumulation and circulation times, poor tumor penetration, and multiple day imaging procedure result in their suboptimal diagnostic accuracy and reduced clinical use.

In contrast, small-molecule probes possess advantages of drug-like pharmacokinetics, high atom-economy, and reduced production costs. To point, Pomper et al. have pioneered the development of small molecule PSMA-targeted PET and SPECT probes to successfully image prostate tumor xenografts in mouse models, using a urea-based peptidomimetic scaffold with avidity for PSMA's active site [15–18]. While the pharmacokinetic and imaging profile with these agents appears more superior to antibody-based approaches, washout of the tracer over several hours was observed [15].

Recently, we demonstrated that our phosphoramidate-based peptidomimetic PSMA inhibitors may be outfitted with imaging payloads without having an adverse effect on their inhibitory capabilities [6,19]. Our lead irreversible phosphoramidate inhibitor 1, with a serine as the P1 residue and glutamate as the P1' residue ($\text{IC}_{50} = 14 \text{ nM}$) (Fig. 1) was modified to selectively deliver the tracer to PSMA(+) cells both *in vitro* and *in vivo*. When conjugated with a fluorescent dye, 1 was found to accumulate in PSMA(+) cells presumably through the internalization of the PSMA enzyme-inhibitor complex [19]. This phosphoramidate inhibitor 1 has also been validated for SPECT and PET imaging of with PSMA(+) cells and tumors when labeled with $^{99\text{m}}\text{Tc}$ and ^{18}F respectively [6,7,20].

In an effort to further our understanding of the phosphoramidate scaffold's binding to PSMA and to improve the overall *in vivo* characteristics for human use, we have structurally modified the scaffold with 2-(3-hydroxypropyl)glycine and aminohexanoate, forming a new

phosphoramidate inhibitor 3 to improve its binding, stability and imaging efficacy. 3 was further appended with a [¹⁹F]-fluorobenzoyl moiety, yielding 5. Herein we report the synthesis, radiolabeling and characterization of [¹⁸F]5 as well as its *in vitro* cell uptake and internalization in PSMA(+) LNCaP and CWR22Rv1 cells and PSMA(-) PC3 cells. Additionally, *in vivo* PET imaging and biodistribution data were obtained in mice implanted with CWR22Rv1 tumor xenografts.

2. Materials and methods

2.1. Cell lines, reagents and general procedures

LNCaP, CWR22Rv1 and PC-3 cells were obtained from the American Type Culture Collection (Manassas, VA). NCr-nu/nu mice (strain code 088) were purchased from Charles River (Hollister, CA). Z-6-Aminohexanoic acid (CBZ-AH-OH) was purchased from Sigma-Aldrich (St. Louis, MO). All chemicals and cell-culture reagents were purchased from Fisher Scientific (Sommerville, NJ) or Sigma-Aldrich. All solvents used in chemical reactions were anhydrous and obtained as such from commercial sources or distilled prior to use. All other reagents were used as supplied unless otherwise stated. Liquid flash chromatography (silica or C18) was carried out using a Flash Plus chromatography system (Biotage, Charlotte, NC). High-resolution mass spectrometry was performed using an ABS 4800 MALDI TOF/TOF Analyzer (Applied Biosystems, Framingham, MA). ESI was performed using API 4000 Electrospray Ionization Triple Quadrupole MS/MS. ¹H NMR chemical shifts were referenced to tetramethylsilane ($\delta = 0.00$ ppm), CDCl₃ ($\delta = 7.26$ ppm) or D₂O ($\delta = 4.87$ ppm). ¹³C NMR chemical shifts were referenced to CDCl₃ ($\delta = 77.23$ ppm). ³¹P NMR chemical shifts in CDCl₃ or D₂O were externally referenced to 85% H₃PO₄ ($\delta = 0.00$ ppm) in CDCl₃ or D₂O. Aqueous buffered solutions for *in vitro* experiments and HPLC chromatography were prepared with deionized distilled water (Milli-Q water system, Millipore, Billerica, MA).

The HPLC analysis and purification system for radioactive compounds were performed on a Waters model 600 Multisolvant System pump equipped with a Shimadzu model SPD-10A UV detector and an in-line radioactivity detector (model 105 s, Carroll and Ramsey Associates, Berkeley, CA) that was coupled to a data collection system (PeakSimple model 304, SRI, Torrance, CA).

2.2. Synthesis of phosphoramidate 3 and its fluorinated analogs

The general synthetic sequence of these compounds is shown in Fig. 2. Syntheses of precursors I and II, their intermediates, and *N*-succinimidy-4-[¹⁸F]fluorobenzoate ([¹⁸F]SFB) and their supporting analysis data are provided in the Supplementary Information (Section 1).

2.2.1. 2-(((S)-((4R)-4-(4-(6-aminohexanamido)-4-carboxybutanamido)-4-carboxybut-oxy)phosphoryl)amino)pentanedioic acid, 3—To a solution of a benzyl ester protected phosphoramidate (II) (0.160 g, 0.124 mmol) in THF (1 mL), was added 10% Pd/C (16 mg), K₂CO₃ (0.044 mg, 0.318 mmol) and H₂O (1 mL). The mixture was stirred vigorously, purged with Ar_(g) and then charged with H_{2(g)} under balloon pressure

overnight at room temperature. The solution was filtered through a 0.2 μm PTFE micropore filtration disk (Whatman). The solvent was removed *in vacuo* to yield 3 as a white solid in 87% yield. ^1H NMR (300 MHz, D_2O): δ 1.23 (m, 3H), 1.48 (m, 6H), 1.74 (m, 4H), 1.80 (m, 1H), 1.98 (m, 4H), 2.15 (m, 4H), 2.86 (t, 4H), 3.34 (m, 1H), 3.56 (dd, 1H), 3.94 (m, 3H). ^{31}P NMR (300 MHz, D_2O): δ 8.42. HR mass spectroscopy: calculated 584.5, found 585.20 (M + H) for $\text{C}_{21}\text{H}_{37}\text{N}_4\text{O}_{13}\text{P}^+$.

2.2.2. 2-(((S)-((4R)-4-carboxy-4-(4-carboxy-4-(6-(4-fluorobenzamido)hexanamido)butanamido)butoxy)(hydroxy)phosphoryl)amino) pentanedioic acid, 5]

—A solution of *N*-Succinimidyl-4-fluorobenzoate (SFB) (31.52 μmol , 1.5 equiv) in 100 μL DMSO was added to a stirred solution of 3 (21.01 μmol , 1 equiv), 160 μL H_2O and 340 μL of 1M KHCO_3 [21]. The reaction mixture was stirred for 6 h in the dark at room temperature. Unreacted 3 was scavenged by adding 25 mg Si-Isocyanate resin (SiliCycle, Inc., Quebec, Canada) with stirring overnight at room temperature. The solution was subsequently centrifuged (7800 rcf, 10min), and the supernatant was lyophilized in a 2 mL microcentrifuge tube. The unreacted and/or hydrolyzed SFB was removed by successively triturating the lyophilized solid with 1 mL portions of DMSO and centrifuging the mixture (16,200 rcf, 1 min) after each wash; this process was repeated 10 times. The resulting solid was dried *in vacuo* providing the desired 4-fluorobenzamido-phosphoramidate 5 in quantitative yield. ^1H NMR (300 MHz, D_2O): δ 1.18 (m, 4H), 1.42 (m, 8H), 1.68 (m, 4H), 1.90 (m, 4H), 2.11 (m, 4H), 3.20 (t, 4H), 3.56 (m, 1H), 3.85 (m, 4H), 3.91 (m, 4H), 6.97–7.06 (m, 4H), 7.52–7.57 (m, 4H). ^{31}P NMR (300MHz, D_2O): δ 8.44. HR mass spectroscopy: calculated 820.31, found 820.4 (M + H), 858.9 (M + K) for $\text{C}_{28}\text{H}_{40}\text{FN}_4\text{O}_{14}\text{P}^+$.

2.2.3. [^{18}F]5—*N*-Succinimidyl-4- ^{18}F fluorobenzoate (^{18}F SFB), prepared in the UCSF cyclotron facility (see Supplementary Information) was coupled to 3 as previously described with minor modifications [6]. 3 (2–3 mg) dissolved in 100 μL of H_2O , 20 μL of 0.1 M K_2CO_3 and 50–100 μL of ^{18}F SFB were added to a one dram vial charged with a stir bar (pH 9.5–10). The coupling reaction took place for 10 minutes at 37 $^\circ\text{C}$. Prior to the *in vitro* and *in vivo* studies, the radioconjugate was purified on semi-preparative RP-HPLC using a Phenomenex C18(2) 100 \AA , 250 \times 10 mm, 5 μ column. Linear gradient (20% to 90% over 22 minutes) of solvent B in solvent A (A: 0.1% formic acid in water; B: 0.1% formic acid in acetonitrile) at a flow rate of 5 mL/min with radio-detection and UV detection at 254 nm. [^{18}F]5 peak was collected and concentrated via C18 Plus SPE method using acetonitrile for elution. The concentrated [^{18}F]5 was brought to dryness under reduced pressure and nitrogen stream and reconstituted in saline (0.9% NaCl) for *in vitro/in vivo* studies. Radiochemical yields ranged between 30 and 50% decay-corrected from [^{18}F]SFB.

2.3. PSMA inhibition assay and reversibility assay

The PSMA inhibition assay and the reversibility assay were performed as previously described with minor modifications [19,22,23]. Detailed description is provided in the Supplementary Information (Section 2).

2.4. Whole cell lysate extraction and western blot analysis

The extraction of PSMA and its analysis by western blot for LNCaP and CWR22Rv1 cells was performed as described previously [24].

2.5. Glutamate carboxypeptidase II expression, purification, crystallization and data collection

Details about PSMA purification, crystallization with 4 and 5 and data collection can be found in the Supplementary Information (Section 3a).

2.5.1. Structure determination and refinement—Structures were determined by the difference Fourier methods using the structure of the PSMA/NAAG complex (PDB entry 3BXM [25]) as the template model. Model building was accomplished using Coot [26], and calculation steps were performed using Refmac 5.1 [27]. The restraints library and the coordinate files for individual inhibitors were prepared using the PRODRG server [28], and the inhibitors/substrates were fitted into the positive electron density map in the final stages of the refinement.

The stereochemical quality of final models was evaluated using MolProbity [29], and the final models, together with experimental amplitudes were deposited in the RCSB Protein Data Bank under entry codes 4JZ0 (PSMA/4; deposited as hGCPII/CTT1055) and 4JYW (PSMA/5; deposited as hGCPII/CTT1057). Data collection and structure refinement statistics are provided in the Supplementary Information (Section 3b, Table S1).

2.6. In vitro cell uptake and internalization studies

LNCaP, CWR22Rv1 and PC-3 cells were cultured in T-75 flasks with complete growth medium (RPMI 1640 containing 10% heat-inactivated fetal calf serum (FBS), 100 units of penicillin and 100 µg/mL streptomycin) in a humidified incubator at 37 °C and 5% CO₂.

The *in vitro* cell uptake studies followed the procedure described in our previous work [22]. Detailed description is provided in Supplementary Information (Section 2).

Internalization studies followed the method described for the *in vitro* cell uptake studies with a minor modification. Detailed description is provided in Supplementary Information (Section 2).

2.7. In vivo PET imaging and biodistribution studies

Six to eight-week-old athymic NCr-nu/nu male mice were purchased from Charles River (Hollister, CA). All animal experiments were conducted in accordance with the UCSF IACUC-approved protocol. [¹⁸F]5 was evaluated *in vivo* using mouse xenografts.

2.7.1. In vivo PET imaging studies—Approximately 10⁶ PSMA+ CWR22Rv1 cells in 50/50 complete medium and matrigel matrix were implanted in the right shoulder of athymic NCr-nu/nu male mice (approximately 8 weeks old) from Charles River (Hollister, CA). Four weeks after implantation, mice with tumors reaching 150 to 300mm³ were anesthetized by isoflurane inhalation and injected with [¹⁸F]5, 150–200 µCi in 250 µL of saline, in a tail

vein. The anesthetized mice were imaged with 10 min acquisition using a microPET/CT imaging system (Inveon, Siemens, Knoxville, TN) at 1 h and 4 h post injection. PET imaging data were acquired in list mode and reconstructed with the iterative OSEM 2-D reconstruction algorithm provided by the manufacturer.

2.7.2. Biodistribution studies—Four to five weeks after CWR22Rv1 cells implantation, tumor-bearing mice were anesthetized by isoflurane inhalation and administered with 35–40 μCi of [^{18}F]5 in 150 μL of saline through tail vein injection. For the blocking study at the 4 h time point, animals ($n=4$) were injected with 250 μg of 1 in 150 μL saline 1 h prior to the injection of [^{18}F]5. At 1 h and 4 h post injection ($n = 4$ for each time point), these mice were euthanized for biodistribution analysis. Blood was collected by cardiac puncture. Major organs (heart, lung, liver, spleen, kidney, muscle, bone and tumor xenografts) were harvested, weighed, and counted in an automated gamma counter (Wizard 2, PerkinElmer, Waltham, MA). The percent injected dose per gram (%ID/g) of tissue was calculated by comparison with standards of known radioactivity. Statistical analysis was performed using two-tailed student t-test (Microsoft Excel Prism software). A p value of <0.05 was considered statistically significant.

3. Results

3.1. Synthesis of cold standards and radiolabeling precursors

3-hydroxypropylglycine was installed as the P1 residue which was then coupled to the P2 residue Cbz-Glu-OH via deprotection of its terminal amine to yield benzyl protected 2 or coupled with Boc-Glu-OH to yield precursor I [30]. I was then N-deprotected, and Cbz-AH-OH (aminohexanoic acid linker) was installed followed by global deprotection to give 3 in 87% yield. The fluorobenzamide (FB) derivative, 5 and [^{18}F]5 were synthesized in quantitative yields via coupling of 3 with respective succinamidyl-4-fluorobenzoates (SFB and [^{18}F] SFB) at pH 10 (Fig. 2).

No decomposition was observed for 2 at pH 3 over 5 h at 25 $^{\circ}\text{C}$, whereas 1 exhibited rapid decomposition at pH 6 (^{31}P NMR spectra for evaluation of pH stability can be found in the Supplementary Information, Section 5). 5 was used as a cold standard for optimizing the reversed phase HPLC conditions to aid in the purification of [^{18}F]5.

3.2. IC_{50} determination and mode of inhibition

The effect of fluorobenzoyl conjugation to the phosphoramidate scaffold on PSMA inhibition was investigated using an HPLC-based assay [23,31,32]. As observed with the earlier-generation analog 1, no loss of inhibitory potency was observed when 3 (19 nM) was converted to 5 (0.4 nM) [6,22]. Additionally, the phosphoramidates 2, 3 and 5 showed irreversible binding to PSMA.

3.3. Crystallization of phosphoramidates 4 and 5 with PSMA

X-ray structures of the PSMA/4 and PSMA/5 complexes at resolution of 1.83 \AA and 1.73 \AA , respectively, were determined using difference Fourier methods.

Placement of both inhibitors within the PSMA-binding pocket can be unambiguously assigned from the electron density map with 5 modeled in two distinct conformations (Fig. 3A). The positioning of the P1' glutamate and phosphoramidate moieties is virtually identical for both the inhibitors 4 and 5, and both functionalities are engaged in the "canonical" set of interactions with PSMA residues (Fig. 3B) [33,34]. However, there are substantial differences in the arrangement of P1 and distal parts (beyond the P1 residue) of inhibitors. The P1 carboxylate of the phosphoramidate 4 is directly bonded to Arg534 (2.7 Å), Arg536 (2.9 Å), and Asn519 (3.0 Å), the P2 carboxylate accepts a hydrogen bond from the hydroxyl group of Tyr234, while the distal fluorobenzoyl moiety is packed against the side chain of Tyr700. In comparison, the P1 carboxylate of the phosphoramidate 5, forms a salt bridge with the guanidinium group of Arg536 (3.1 and 3.1 Å) and is also engaged in several water-mediated contacts with the side chains of Arg536, Glu457, Arg534, Asn519, and Asp453. Other non-carbon atoms of the 20 Å linker donate or accept a multitude of hydrogen bonds to/from water molecules filling the entrance funnel. Additionally, the main-chain carbonyl accepts hydrogen bond from the guanidinium group of Arg463 (2.8 Å), while the P2 carboxylate is hydrogen bonded to the amide group of the Asn698 side chain (2.9 Å; Supplementary Information, Section 3c). The distal (P2) part of the linker connecting the terminal fluoro-benzoyl moiety, is present in two distinct conformations.

Most importantly, the terminal fluoro-benzoyl functionality (also in two overlapping conformations) is inserted into the arene-binding cleft located at the "entrance lid" of the enzyme (Fig. 3B) [35,36].

The plane of the fluoro-benzoyl ring is virtually parallel to both indole and guanidinium groups of Trp541 and Arg511, respectively, of the arene-binding cleft, and these two functionalities likely contribute considerably to the overall inhibitor binding.

3.4. In vitro uptake and internalization study

The western blot analysis confirmed nearly 5-fold greater PSMA expression in the LNCaP cells as compared to the CWR22Rv1 cells (Supplementary Information, Section 4). This difference in PSMA expression levels between the two cell lines was also mirrored in the cell uptake of [¹⁸F]5. There was a 9.8-fold and 6.6-fold higher cell uptake for LNCaP cells as compared to the CWR22Rv1 cells, at 1 h and 4 h respectively (Table 1). Increased cell uptake in both the cell lines was observed over 4 h incubation with [¹⁸F]5 (Table 1). The percent uptake in LNCaP cells showed about 1.5-fold enhancement while CWR22Rv1 cells showed a 2-fold increased uptake from 1 hr to 4 h. Insignificant uptake for PC-3 cells was observed at both 1 and 4 h.

The internalization of [¹⁸F]5 in LNCaP cells was 93% at 1 h and 92% at 4 h (Table 1). The CWR22Rv1 cells, which have been used as tumor xenografts for *in vivo* imaging and biodistribution, showed 81% and 91% internalization at 1 h and 4 h respectively.

3.5. In vivo imaging and biodistribution study

As shown in Fig. 4, the uptake of [¹⁸F]5 was clearly observed in the PSMA(+) CWR22Rv1 tumors 1 h post-injection. There was significant uptake in the kidneys with clearance mainly

through the bladder with limited accumulation observed in other major organs. The uptake of [^{18}F]5 in the tumor remained the same level even at 4 h post injection while the uptake of other organs diminished. No change was observed in the tracer uptake in the kidney at 1 h and 4 h. The percent radioactivity in bone remained minimal.

The *ex vivo* biodistribution data confirmed the imaging findings (Table 2 and Fig. 5). There was rapid uptake of the tracer in the PSMA positive tumor within the first hour with significant clearance from the blood and other non-PSMA tissues over the 4 h study. At 1 h post-injection, the PSMA(+) tumor accumulation was 2.35 ± 0.91 %ID/g with a tumor-to-blood ratio of 22:1. At 4 h post-injection, the tumor accumulation remained at 2.33 ± 0.50 %ID/g while more than 10-fold clearance from the blood provided a tumor-to-blood ratio of 265:1. The kidneys showed expected high uptake and retention of the tracer with 18.12 ± 2.21 %ID/g and 17.17 ± 4.13 %ID/g at 1 h and 4 h, respectively. Competition study with cold phosphoramidate 1 injected an hour prior to the administration of [^{18}F]5 showed significant decreased in kidney and tumor uptake by 67% ($p=0.0010$) and 91% ($p=0.0003$), respectively.

4. Discussion

The first generation ^{18}F -labeled phosphoramidate inhibitor, 1, has previously demonstrated desirable PSMA targeting properties *in vitro* in LNCaP cells and *in vivo* in LNCaP xenografts. In this work, we have improved the acid-stability of the scaffold by incorporation of a P1 2-(3-hydroxypropyl)glycine residue. We hypothesize that the installation of 2 extra methylene units in the P1 residue of 2 as compared to 1 prevents the collapse of the phosphoramidate by release of P1' glutamate due to protonation of the amine at physiological pH. This provided greater acid stability to 2 compared to 1 and aided purification of the radiolabeled analog *via* the use of acid modifiers in the HPLC mobile phase. Further molecular elaboration off the P2 amino group with the aminohexanoic linker and fluorobenzoylation of the terminal amine using SFB gave 5, which displayed high affinity for PSMA. As observed in the case of 4, functionalization *via* the N-terminal amine of the core phosphoramidate causes no loss of inhibition, and these modified inhibitors still maintain an irreversible mode of binding for PSMA.

The synthetic procedure is highly translatable to routine procedures and scale-ups. Preparation of SFB can be easily achieved using several automated synthesis units and commercially available cassettes. The single step addition of SFB to 3, to generate the desired agent, may be performed at room temperature, and has high coupling yields. In a pre-IND discussion with the FDA regarding the first-in-man studies with [^{18}F]5, the FDA did not raise any concerns about the non-traditional prosthetic labeling approach for this radiotracer.

To gather insight into the modes of interaction of 5 with PSMA and compare it with our previous agent 4, both compounds were co-crystallized with the extracellular domain of PSMA. Co-crystallization of 5 with PSMA revealed several additional interactions that may contribute toward its enhanced affinity towards PSMA, as compared to analog 4. Apart from many pronounced interactions of the P1/P2 residues of 5 with the enzyme, a multitude of H-

bonds is formed with the non-carbon atoms of the 20 Å AH linker within the entrance funnel. It is interesting to note that the conformation of the Arg536 side chain in the PSMA/5 complex differs from “typical” conformations of this “invariable” arginine observed in complexes reported previously [34,35], most likely due to “the pulling effect” of the P1 carboxylate. The most prominent interaction however, was the π -stacking, π -cationic interaction of the fluorobenzamido ring with the Arg511/Trp541 and Arg 463 residues respectively, known as the arene-binding cleft located at the entrance lid of the protein, behaving in a bidentate fashion and contributing considerably to the overall affinity and irreversibility of 5. This observation mirrors similar finding for GCPII/ARM-P complexes [36]. Although differing in both the linker length and the chemistry of their distal groups, binding modes of 5 and ARM-P are very similar, strengthening the notion of the arene-binding cleft as a “universal” structural motif exploitable for the design of bidentate GCPII inhibitors.

In vitro cell uptake experiments showed elevated uptake of [¹⁸F]5 in the PSMA(+), LNCaP and CWR22Rv1 cells compared to the PSMA(–) PC3 cells. The low uptake in PC-3 cells was expected due to absence of PSMA expression in the cell line [37]. There was also a significantly greater uptake in the LNCaP cells compared to the CWR22Rv1 cells, consistent with the known 3- to 5-fold higher concentration of PSMA in LNCaP cells, which was further confirmed by western blot experiments. The [¹⁸F]5 rapidly internalized in both PSMA(+) cell types with more than 80% of the compound associated with CWR22Rv1 cells and more than 90% with LNCaP cells at 1 h. These internalization values were much higher than what has been typically known for the reported urea-based agents [38], presumably due to the irreversible binding of the phosphoramidates [19,22]. Based on these observations, it was expected that *in vivo* tumor uptake of the radiotracer would occur shortly after administration, retain within the tumor over several hours, and develop greater contrast with the background tissues.

Even though the LNCaP cell line, used in the study of our first generation analog [¹⁸F]4, exhibits greater PSMA expression, its growth rate and proliferation as tumor xenografts in animal models is unpredictable and often leads to tumor necrosis. In contrast, CWR22Rv1 cell lines have moderate PSMA expression but are predictable in their growth as tumor xenografts. In addition, the cellular PSMA concentration in the CRW22Rv1 cells is more akin to the expression levels expected in human prostate cancer metastases. Therefore, for the *in vivo* studies, the mice were implanted with CWR22Rv1 xenografts. Imaging and bio-distribution was performed at 1 and 4 h post-injection of [¹⁸F]5, in contrast to the 2 h post-injection study performed in the case of our previous agent [¹⁸F]4. While there cannot be a head-to-head comparison, since the studies of the two compounds occur at different time points and tumor types (LNCaP vs. CWR22Rv1), they inform the reader of an overall trend in the uptake and clearance of the radiotracers.

The overall pharmacokinetics of [¹⁸F]4 and [¹⁸F]5 are comparable with very low non-target uptake, with the exception of the kidneys. The elevated kidney uptake was expected due to the known high PSMA expression in the mouse kidneys, an artifact of this animal model [39]; and thus can be treated as a good secondary indicator of PSMA specificity. The kidney uptake was for [¹⁸F]5 was about 7-fold greater at 1 h compared to [¹⁸F]4 at 2 h, presumably

due to [^{18}F]5's greater affinity for PSMA. The tumor-to-blood ratio for [^{18}F]5 at 1 h (22:1) was also significantly higher than [^{18}F]4 at 2 h (9:1), and this ratio for [^{18}F]5 increased to 265:1 at 4 h. Also, the tumor uptake for [^{18}F]4 was 1.24% at 2 h in the LNCaP tumor, as compared to 2.35% for [^{18}F]5 at 1 h in CW22Rv1 tumor, with continued retention at 4 h (2.33%). The irreversible mode of binding of [^{18}F]5, possibly contributes to its tumor retention, in contrast to the washout that is reported over time for most urea-based agents [38]. Keeping in mind the higher PSMA expression in the LNCaP tumors used for [^{18}F]4, these compelling results are indicative of much higher binding, retention and contrast for [^{18}F]5.

Competition studies by pre-injection of 1 to block the binding pockets on PSMA before [^{18}F]5 was injected showed reduced uptake in the tumor, indicating [^{18}F]5 to be a PSMA-specific targeting ligand. It is important to point out that no defluorination of the compound 5 was observed throughout, which was indicated by the insignificant bone uptake.

In conclusion, we have successfully demonstrated [^{18}F]fluorobenzamido-amino-hexanoic-phosphoramidate [^{18}F]5 is a promising PET imaging agent for targeting PSMA in prostate cancer. With its exceptional binding, tumor uptake and retention, remarkable tumor-to-blood ratios, and a high yielding synthesis, that is amenable for reproducible preparation, it is positioned as a promising candidate for forthcoming clinical trials.

Supplementary Material

Refer to Web version on PubMed Central for supplementary material.

Acknowledgments

This work was supported in part by the National Institutes of Health (R01 CA140617) and the Department of Defense (W81XWH-11-1-0464). The authors extend their gratitude for technical assistance to G. Helms and W. Hiscox (WSU Center for NMR Spectroscopy), Gerhard Munske (WSU lab Bioanalysis and Biotechnology for mass spectrometry), Dr. Jacek Lubkowski and Dr. Manfred Weiss (crystal structure data collection). We thank *Helmholtz-Zentrum Berlin* and *the Advanced Photon Source, Argonne National Laboratory* for the allocation of synchrotron radiation beamtime at beamlines MX14.2 and SER-CAT 22-ID, respectively. The research leading to these results has received funding from the European Community's Seventh Framework Programme (FP7/2007-2013) under BioStruct-X (grant agreement N°283570) and the U.S. Department of Energy, Office of Science, Office of Basic Energy Sciences, under Contract No. W-31-109-Eng-38. C.B. acknowledges the support from the Czech Science Foundation (grant No 301/12/1513). This publication is supported by the project BIOCEV (CZ.1.05/1.1.00/02.0109) from the ERDF. The authors also thank Dr. Lisa Wu for her helpful comments on this manuscript.

References

1. Chang SS, O'Keefe DS, Bacich DJ, Reuter VE, Heston WD, Gaudin PB. Prostate-specific membrane antigen is produced in tumor-associated neovasculature. *Clin Cancer Res.* 1999; 5(10): 2674–81. [PubMed: 10537328]
2. Rosenthal SA, Haseman MK, Polascik TJ. Division of radiation oncology RAoSMGICUSA. Utility of capromab pendetide (ProstaScint) imaging in the management of prostate cancer. *Tech Urol.* 2001; 7(1):27–37. [PubMed: 11272670]
3. Bander NH, Milowsky MI, Nanus DM, Kostakoglu L, Vallabhajosula S, Goldsmith SJ. Phase I trial of 177 lutetium-labeled J591, a monoclonal antibody to prostate-specific membrane antigen, in patients with androgen-independent prostate cancer. *J Clin Oncol.* 2005; 23:4591–601. [PubMed: 15837970]

4. Foss CA, Mease RC, Fan H, Wang Y, Ravert HT, Dannals RF, et al. Radiolabeled small-molecule ligands for prostate-specific membrane antigen: in vivo imaging in experimental models of prostate cancer. *Clin Cancer Res*. 2005; 11:4022–8. [PubMed: 15930336]
5. Pomper MG, Musachio JL, Zhang J, Scheffel U, Zhou Y, Hilton J, et al. 11C-MCG: synthesis, uptake selectivity, and primate PET of a probe for glutamate carboxypeptidase II (NAALADase). *Mol Imaging*. 2002; 1:96–101. [PubMed: 12920850]
6. Lapi SE, Wahnische H, Pham D, Wu LY, Nedrow-Byers JR, Liu T, et al. Assessment of an 18 F-labeled phosphoramidate peptidomimetic as a new prostate-specific membrane antigen-targeted imaging agent for prostate cancer. *J Nucl Med*. 2009; 50:2042–8. [PubMed: 19910433]
7. Nedrow-Byers JR, Jabbes M, Jewett C, Ganguly T, He H, Liu T, et al. A phosphoramidate-based prostate-specific membrane antigen-targeted SPECT agent. *Prostate*. 2012; 72:904–12. [PubMed: 22670265]
8. Tasch J, Gong M, Sadelain M, Heston WD. Department of Urology MHMS-KCCNYUSA. A unique folate hydrolase, prostate-specific membrane antigen (PSMA): a target for immunotherapy? *Crit Rev Immunol*. 2001; 21(1–3):249–61. [PubMed: 11642607]
9. Fracasso G, Bellisola G, Cingarlini S, Castelletti D, Prayer-Galetti T, Pagano F, et al. Anti-tumor effects of toxins targeted to the prostate specific membrane antigen. *Prostate*. 2002; 53(1):9–23. [PubMed: 12210476]
10. Liu T, Wu LY, Choi JK, Berkman CE. Targeted photodynamic therapy for prostate cancer: inducing apoptosis via activation of the caspase-8/-3 cascade pathway. *Int J Oncol*. 2010; 36:777–84. [PubMed: 20198319]
11. Elsasser-Beile U, Buhler P, Wolf P. Targeted therapies for prostate cancer against the prostate specific membrane antigen. *Curr Drug Targets*. 2009; 10:118–25. [PubMed: 19199907]
12. Nanus DM, Milowsky MI, Kostakoglu L, Smith-Jones PM, Vallabahajosula S, Goldsmith SJ, et al. Clinical use of monoclonal antibody HuJ591 therapy: targeting prostate specific membrane antigen. *J Urol*. 2003; 170:S84–8. discussion S8–9. [PubMed: 14610416]
13. Bander NH, Nanus DM, Milowsky MI, Kostakoglu L, Vallabahajosula S, Goldsmith SJ. Targeted systemic therapy of prostate cancer with a monoclonal antibody to prostate-specific membrane antigen. *Semin Oncol*. 2003; 30:667–76. [PubMed: 14571414]
14. Holland JP, Divilov V, Bander NH, Smith-Jones PM, Larson SM, Lewis JS. 89Zr-DFO-J591 for ImmunoPET of prostate-specific membrane antigen expression in vivo. *J Nucl Med*. 2010; 51:1293–300. [PubMed: 20660376]
15. Mease RC, Dusich CL, Foss CA, Ravert HT, Dannals RF, Seidel J, et al. N-[N-[(S)-1,3-Dicarboxypropyl]carbamoyl]-4-[18 F]fluorobenzyl-L-cysteine, [18 F]DCFBC: a new imaging probe for prostate cancer. *Clin Cancer Res*. 2008; 14:3036–43. [PubMed: 18483369]
16. Banerjee SR, Foss CA, Castanares M, Mease RC, Byun Y, Fox JJ, et al. Synthesis and evaluation of technetium-99 m- and rhenium-labeled inhibitors of the prostate-specific membrane antigen (PSMA). *J Med Chem*. 2008; 51:4504–17. [PubMed: 18637669]
17. Molecular insight pharmaceuticals presents clinical oncology data at Society of Nuclear Medicine 2012 Annual Meeting 2012
18. Banerjee SR, Pullambhatla M, Byun Y, Nimmagadda S, Green G, Fox JJ, et al. 68Ga-labeled inhibitors of prostate-specific membrane antigen (PSMA) for imaging prostate cancer. *J Med Chem*. 2010; 53:5333–41. [PubMed: 20568777]
19. Liu T, Wu LY, Kazak M, Berkman CE. Cell-Surface labeling and internalization by a fluorescent inhibitor of prostate-specific membrane antigen. *Prostate*. 2008; 68:955–64. [PubMed: 18361407]
20. Nedrow-Byers JR, Moore AL, Ganguly T, Hopkins MR, Fulton MD, Benny PD, et al. PSMA-targeted SPECT agents: mode of binding effect on in vitro performance. *Prostate*. 2013; 73:355–62. [PubMed: 22911263]
21. Murthy JNH, Jocelyn M, Soldin Steven J. Evaluation of i-STAT portable clinical analyzer in a neonatal and pediatric intensive care unit. *Clin Biochem*. 1997; 30(5):385–9. [PubMed: 9253514]
22. Liu T, Toriyabe Y, Kazak M, Berkman CE. Pseudoirreversible inhibition of prostate-specific membrane antigen by phosphoramidate peptidomimetics. *Biochemistry*. 2008; 47:12658–60. [PubMed: 18983168]

23. Wu LY, Anderson MO, Toriyabe Y, Maung J, Campbell TY, Tajon C, et al. The molecular pruning of a phosphoramidate peptidomimetic inhibitor of prostate-specific membrane antigen. *Bioorg Med Chem.* 2007; 15:7434–43. [PubMed: 17869524]
24. Liu T, Wu LY, Berkman CE. Prostate-specific membrane antigen-targeted photodynamic therapy induces rapid cytoskeletal disruption. *Cancer Lett.* 2010; 296:106–12. [PubMed: 20452720]
25. Klusak V, Barinka C, Plechanovova A, Mlcochova P, Konvalinka J, Rulisek L, et al. Reaction mechanism of glutamate carboxypeptidase II revealed by mutagenesis, X-ray crystallography, and computational methods. *Biochemistry.* 2009; 48:4126–38. [PubMed: 19301871]
26. Emsley P, Lohkamp B, Scott WG, Cowtan K. Features and development of Coot. *Acta Crystallogr D Biol Crystallogr.* 2010; 66:486–501. [PubMed: 20383002]
27. Murshudov GN, Skubak P, Lebedev AA, Pannu NS, Steiner RA, Nicholls RA, et al. REFMAC5 for the refinement of macromolecular crystal structures. *Acta Crystallogr D Biol Crystallogr.* 2011; 67:355–67. [PubMed: 21460454]
28. Schuttelkopf AW, van Aalten DM. PRODRG: a tool for high-throughput crystallography of protein-ligand complexes. *Acta Crystallogr D Biol Crystallogr.* 2004; 60:1355–63. [PubMed: 15272157]
29. Chen VB, Arendall WB III, Headd JJ, Keedy DA, Immormino RM, Kapral GJ, et al. MolProbity: all-atom structure validation for macromolecular crystallography. *Acta Crystallogr D Biol Crystallogr.* 2010; 66:12–21. [PubMed: 20057044]
30. Martin SE, Ganguly T, Munske GR, Fulton MD, Hopkins MR, Berkman CE, et al. Development of inhibitor-directed enzyme prodrug therapy (IDEPT) for prostate cancer. *Bioconjug Chem.* 2014; 25:1752–60. [PubMed: 25157916]
31. Maung J, Mallari JP, Girtsman TA, Wu LY, Rowley JA, Santiago NM, et al. Probing for a hydrophobic a binding register in prostate-specific membrane antigen with phenylalkylphosphonamidates. *Bioorg Med Chem.* 2004; 12:4969–79. [PubMed: 15336276]
32. Anderson MO, Wu LY, Santiago NM, Moser JM, Rowley JA, Bolstad ES, et al. Substrate specificity of prostate-specific membrane antigen. *Bioorg Med Chem.* 2007; 15:6678–86. [PubMed: 17764959]
33. Barinka C, Rovenska M, Mlcochova P, Hlouchova K, Plechanovova A, Majer P, et al. Structural insight into the pharmacophore pocket of human glutamate carboxypeptidase II. *J Med Chem.* 2007; 50:3267–73. [PubMed: 17567119]
34. Pavlicek J, Ptacek J, Barinka C. Glutamate carboxypeptidase II: an overview of structural studies and their importance for structure-based drug design and deciphering the reaction mechanism of the enzyme. *Curr Med Chem.* 2012; 19:1300–9. [PubMed: 22304708]
35. Barinka C, Hlouchova K, Rovenska M, Majer P, Dauter M, Hin N, et al. Structural basis of interactions between human glutamate carboxypeptidase II and its substrate analogs. *J Mol Biol.* 2008; 376:1438–50. [PubMed: 18234225]
36. Zhang AX, Murelli RP, Barinka C, Michel J, Cocleaza A, Jorgensen WL, et al. A remote arene-binding site on prostate specific membrane antigen revealed by antibody-recruiting small molecules. *J Am Chem Soc.* 2010; 132:12711–6. [PubMed: 20726553]
37. Liu T, Wu LY, Fulton MD, Johnson JM, Berkman CE. Prolonged androgen deprivation leads to downregulation of androgen receptor and prostate-specific membrane antigen in prostate cancer cells. *Int J Oncol.* 2012; 41:2087–92. [PubMed: 23041906]
38. Hillier SM, Maresca KP, Femia FJ, Marquis JC, Foss CA, Nguyen N, et al. Preclinical evaluation of novel glutamate-urea-lysine analogues that target prostate-specific membrane antigen as molecular imaging pharmaceuticals for prostate cancer. *Cancer Res.* 2009; 69:6932–40. [PubMed: 19706750]
39. Aggarwal S, Ricklis RM, Williams SA, Denmeade SR. Comparative study of PSMA expression in the prostate of mouse, dog, monkey, and human. *Prostate.* 2006; 66:903–10. [PubMed: 16496413]

Appendix A. Supplementary data

Supplementary data to this article can be found online at <http://dx.doi.org/10.1016/j.nucmedbio.2015.06.003>.

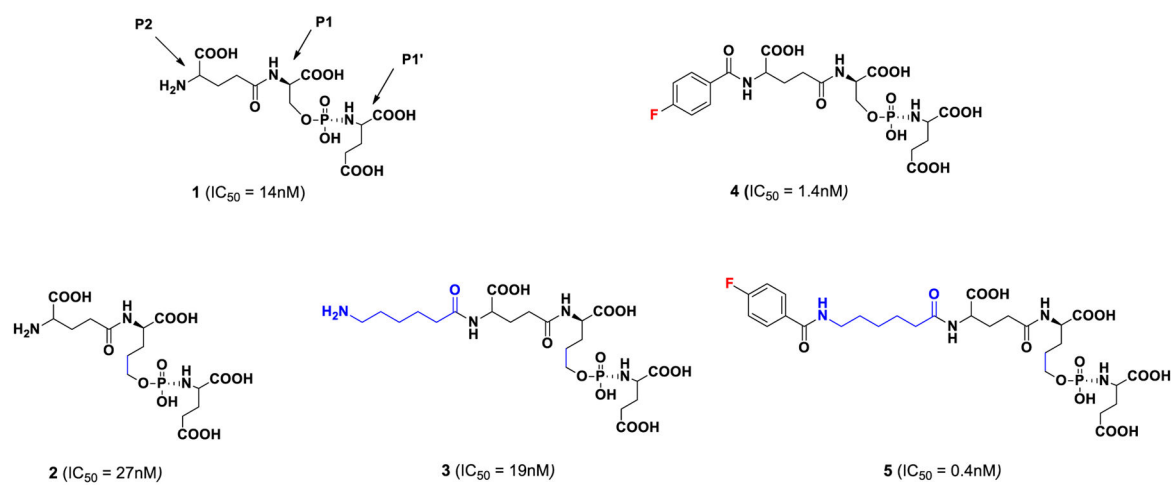


Fig. 1.
Irreversible phosphoramidate analogs. The P1', P1 and P2 residues for a typical phosphoramidate scaffold have been designated.

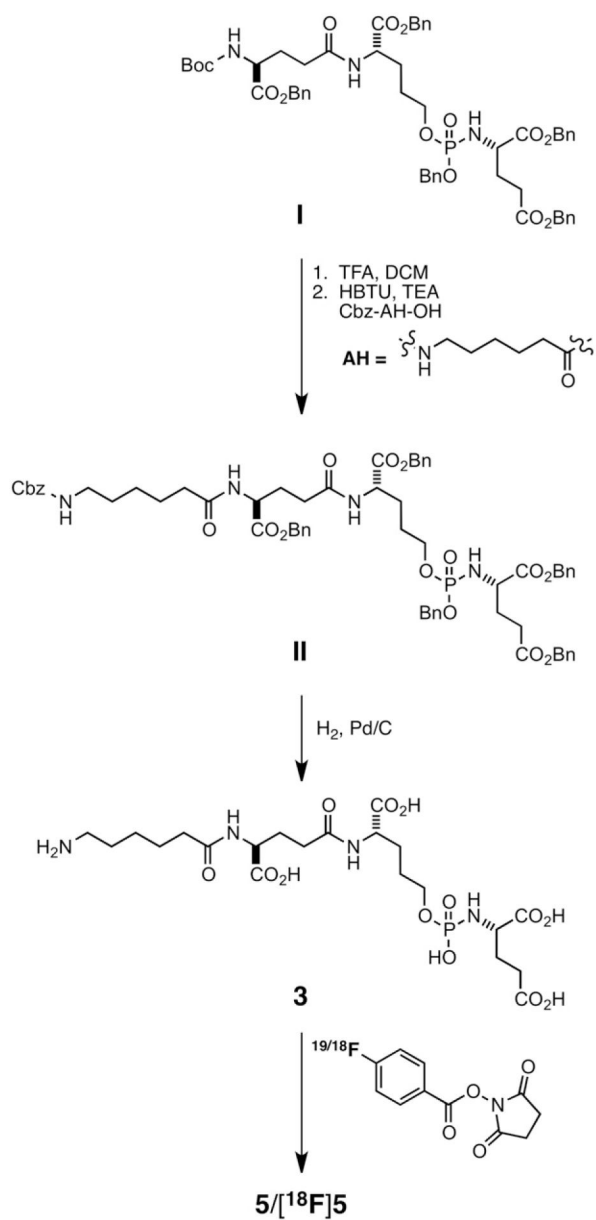


Fig. 2. Synthetic scheme for **3** and its fluorinated analogs.

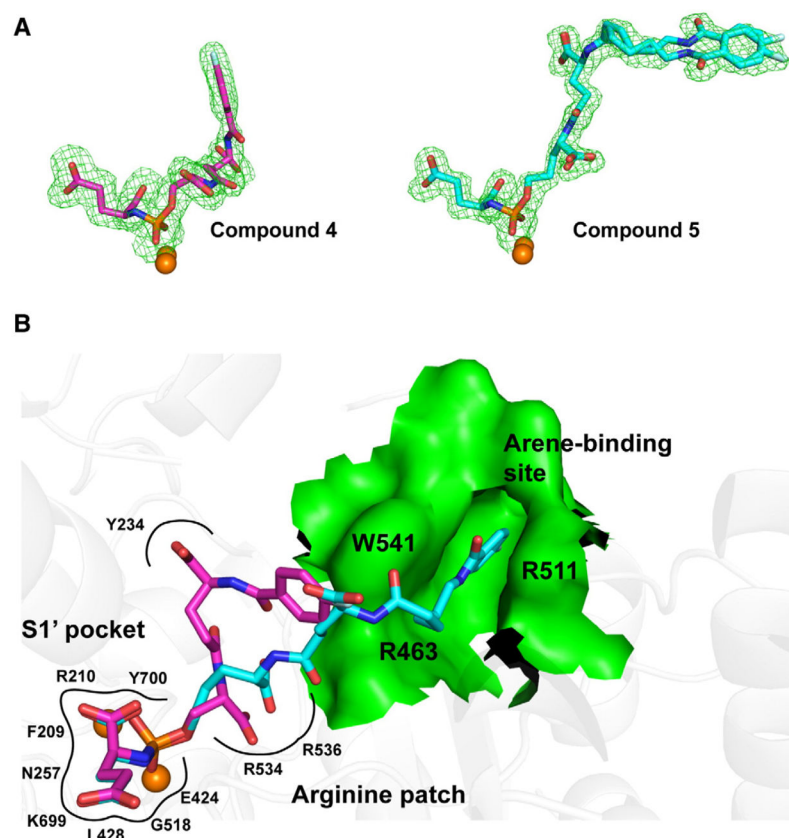


Fig. 3. Crystal structures of 4 and 5 in complex with PSMA (PDB codes 4JZ0 and 4JYW respectively). Panel A: Difference F_o-F_c maps (green) for individual inhibitors are contoured at 3.0σ , and modeled inhibitors are shown in stick representation with atoms colored magenta (carbon, compound 4), cyan (carbon, compound 5), red (oxygen), blue (nitrogen), orange (phosphorus), and palecyan (fluorine). The active-site zinc ions are shown as orange spheres. Panel B: The superposition of the active-site bound inhibitors. Complexes of PSMA/inhibitor were superimposed on corresponding Ca atoms of the enzyme. Superposed inhibitors are shown in stick representation with carbons of 4 and 5 colored magenta and cyan, respectively. Zinc ions are shown as orange spheres, and PSMA is shown in cartoon representation (gray). The arene-binding site (ABS) is highlighted in surface representation and colored green. Notice the positioning of the distal part of 5 inside the ABS groove allowed for by the longer linker.

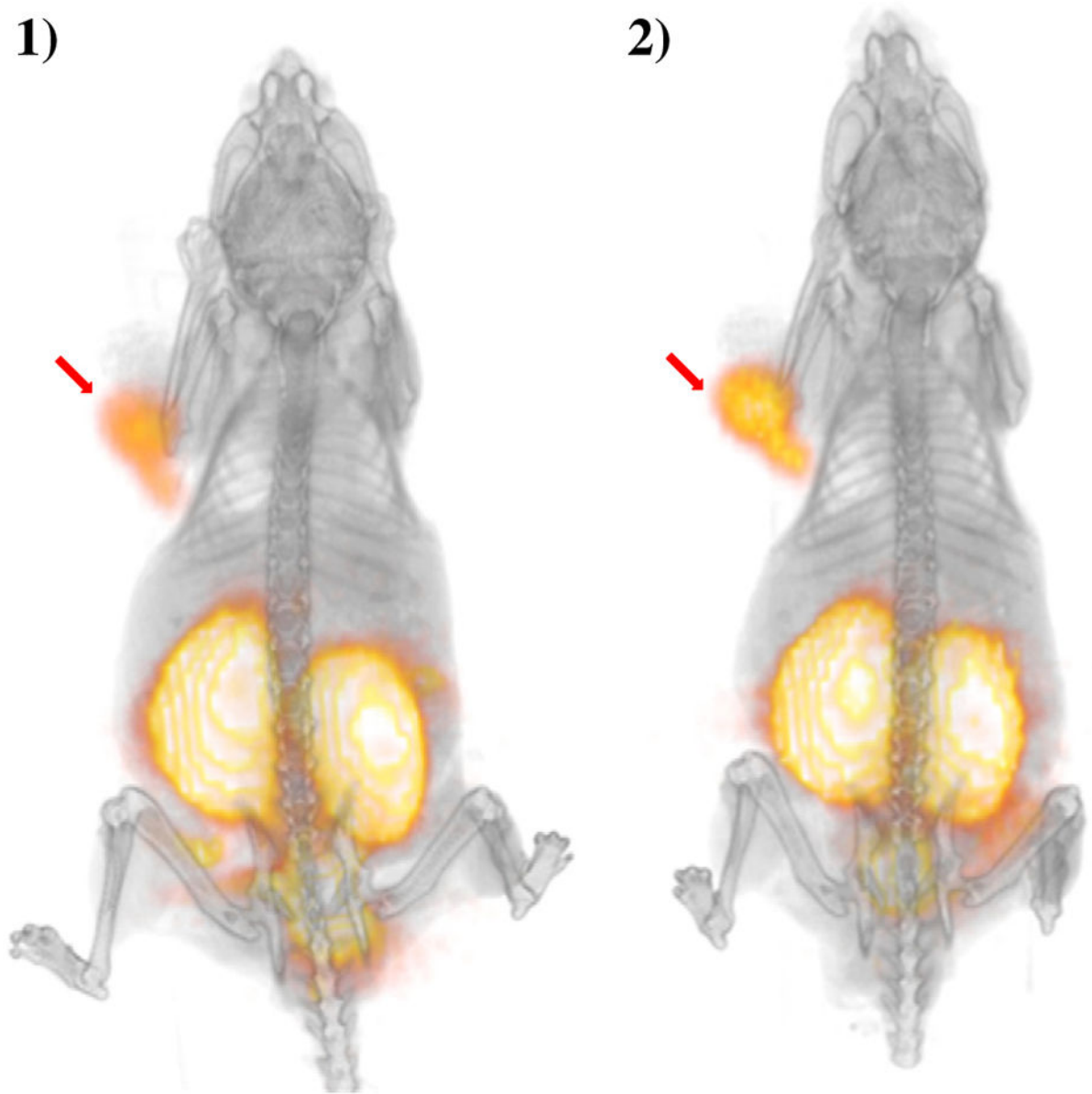


Fig. 4. PET dorsal images of male nude mice bearing CWR22Rv1 tumor xenografts 1) 1 h and 2) 4 h pi of [^{18}F]5 (150–200 μCi in 250 μL of saline). The mouse was anesthetized by isoflurane inhalation, and was imaged with 10 min acquisition using a microPET/CT imaging system. Arrows include tumor placement.

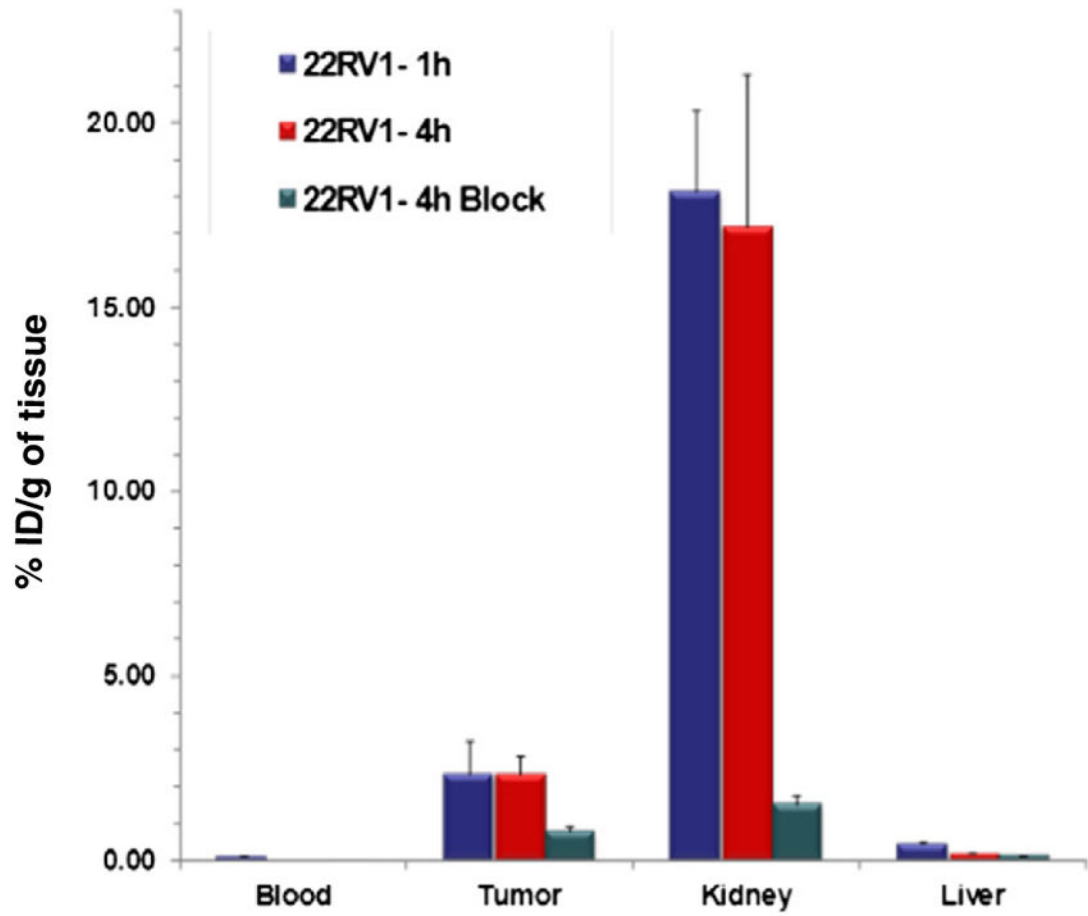


Fig. 5. Biodistribution of $[^{18}\text{F}]5$ in CWR22Rv1-bearing mice (n=4 in each group). Tissues were harvested at 1 h, 4 h post tracer injection. Blocking was achieved by injection of 1, 1 h prior to $[^{18}\text{F}]5$ injection.

Table 1Percent cell uptake and percent internalization data for [¹⁸F]5 in PSMA(+) and PSMA(-) cell lines.

Cell line	% Uptake		% Internalization	
	1h ^a	4h ^a	1h ^a	4h ^a
CWR22Rv1	0.56 ± 0.05	1.32 ± 0.52	81.4 ± 2.7 [†]	90.7 ± 2.7 [†]
LNCaP	5.51 ± 0.77	8.74 ± 2.67	92.9 ± 0.7*	92.1 ± 0.7*
PC3	0.04 ± 0.01	0.04 ± 0.01	ND	ND

^a n = 3; mean ± standard deviation.

Author Manuscript

Author Manuscript

Author Manuscript

Author Manuscript

Table 2Complete *ex vivo* biodistribution data for [¹⁸F]5 (n = 4, average ± standard deviation).

Tissue	1 h	4 h	4 h blocked
Blood	0.104 ± 0.025	0.011 ± 0.007	0.004 ± 0.001
Heart	0.311 ± 0.044	0.067 ± 0.010	0.039 ± 0.006
Lung	0.341 ± 0.052	0.159 ± 0.037	0.050 ± 0.005
Liver	0.451 ± 0.061	0.167 ± 0.045	0.129 ± 0.008
Kidney	18.123 ± 2.202	17.192 ± 4.132	1.489 ± 0.268
Spleen	0.819 ± 0.192	0.401 ± 0.135	0.275 ± 0.065
Bone	0.193 ± 0.080	0.050 ± 0.008	0.041 ± 0.007
Muscle	0.112 ± 0.030	0.036 ± 0.014	0.013 ± 0.002
Tumor	2.350 ± 0.910	2.334 ± 0.504	0.771 ± 0.141
Tumor:Blood	21.98 ± 4.17	265.39 ± 136.32	180.85 ± 34.90

Author Manuscript

Author Manuscript

Author Manuscript

Author Manuscript